Inorganica Chimica Acta, *124* (1986) 13–28

Biochemical Effects of Binding $[(H_2O)(NH_3)_5Ru^{II}]^{2+}$ to DNA and Oxidation to $[(NH_3)_5Ru^{III}]_n$–DNA

MICHAEL J. CLARKE*, BRUCE JANSEN

Department of Chemistry, Boston College, Chestnut Hill, Mass. 02167, U.S.A.

KENNETH A. MARX* and RAY KRUGER

Department of Chemistry, Dartmouth College, Hanover, N.H. 03755, U.S.A.

Received October 24, 1985

Abstract

The reaction of $[(H_2O)(NH_3)_5Ru^{II}]^{2+}$ with calf thymus and salmon sperm DNA has been studied over a wide range of transition metal ion concentrations. Kinetic studies revealed a biphasic reaction with an initial fairly rapid coordination of the metal ion being followed by slower reactions. Binding studies were done under pseudo-equilibrium conditions following completion of the initial rapid reaction. Spectra and HPLC of acid-hydrolyzed samples of $[(NH_3)_5Ru^{III}]_n$–DNA prepared by incubation of $[(H_2O)(NH_3)_5Ru^{II}]^{2+}$ with DNA (where $[P_{DNA}] = 1.5$ mM and reactant $[Ru^{II}]/[P_{DNA}]$ ratios were in the range 0.1 to 0.3) followed by air oxidation showed the predominant binding site on helical DNA to be in the major groove at the N-7 of guanine. The equilibrium constant for $[(H_2O)(NH_3)_5Ru^{II}]^{2+}$ binding to the G^7 site in helical CT DNA is 5.1×10^3. Differential pulse voltammetry exhibited a single peak at 48 mV, which is attributed to the reduction of Ru^{III} on the G^7 sites.

At $[Ru^{II}]/[P_{DNA}] \leqslant 0.5$, T_m values for the DNA decreased linearly with increasing ruthenium concentration and an increase in the intensity of the 565 nm $dG \rightarrow Ru(III)$ charge transfer band was noted upon melting. The UV and CD spectra of these samples indicated no extensive destacking or alteration in geometry (B family) compared to unsubstituted DNA. At $[Ru^{II}]/[P_{DNA}] > 0.5$ or when single-stranded DNA was used, increased absorbance at 530 nm and 480 nm suggested additional binding to the exocyclic amine sites of adenine and cytosine residues. HPLC and individual spectrophotometric identification of the products derived from hydrolysis of these species yielded both $[(Gua)(NH_3)_5Ru^{III}]$ and $[(Ade)(NH_3)_5Ru^{III}]$. Earlier studies have established the cytidine and adenosine binding sites of $[(NH_3)_5Ru^{III}]$ to be at their exocyclic amines (C^4 and A^6). Coordination to these positions indicates disruption of the double helix since these amines are involved in hydrogen bonding on the interior of B-DNA.

Agarose gel electrophoresis of superhelical pBR322 plasmid DNA after exposure to various complexes of $[(NH_3)_5Ru^{III}]$ in the presence of a reductant and air generally revealed moderately efficient cleavage of the DNA, presumably due to the generation of hydroxyl radical via Fenton's chemistry. However, similar studies involving $[(NH_3)_5Ru^{III}]$ directly coordinated to the DNA showed no strand cutting above background. Polyacrylamide gel electrophoresis of a 381 bp, $3'$-^{32}P-labeled fragment of pBR322 plasmid DNA containing low levels of bound $[(NH_3)_5Ru^{III}]$ further indicated negligible DNA cutting by the coordinated metal ion.

Introduction

A number of ammineruthenium complexes have shown good antitumor activity [1, 2] and are currently under consideration for new drug development [3]. *In vitro* biochemical studies demonstrate that Ru^{II} and Ru^{III} compounds are active in inhibiting DNA synthesis and possess mutagenic activity in the Ames and related assays [4–6]. Ammineruthenium(III) ions are also potentially useful as paramagnetic probes of metal ion interactions with DNA and have been used as heavy-atom markers for X-ray structure determinations of nucleic acids [7]. It has also been suggested recently that ruthenium complexes with bipyridine ligands intercalate into DNA prior to covalently binding to guanine residues [8].

Ruthenium is a platinum group metal, which occurs in aqueous solution predominantely as Ru^{II} and Ru^{III}. Ruthenium ions in these oxidation states are invariably six-coordinate with octahedral geometry and are generally inert to substitution when bound to nitrogen bases [9]. The loss of ammines and heterocyclic nitrogen bases from $[L(NH_3)_5Ru^{II}]$

*Authors to whom correspondence should be addressed.

0020-1693/86/$3.50

(where L = NH_3 or nitrogen heterocycle) is usually faster than in corresponding Ru(III) complexes, but still proceeds fairly slowly, with half-lives on the order of a day under physiological conditions [10].

Preliminary studies of the binding of ammineruthenium ions to DNA [11] indicate that advantage can be taken of their intertness to ligand substitution to establish DNA coordination sites. Once coordinated to a nitrogen base, either Ru^{II} or Ru^{III} usually remains bound to the same base, if not to the same atom on the base [9, 10, 12]. Thus, determining the coordination site for $[(NH_3)_5Ru^{III}]$ is usually sufficient to also establish base coordination for the lower valent state. However, as will be pointed out in the discussion, these coordination site assignments must be made with care, since metal ion migration can occur under appropriate conditions following changes in the metal ion oxidation state.

In both their initial DNA binding site and in the oncological consequences of their DNA interactions, ammineruthernium complexes resemble *cis*-$[Cl_2(NH_3)_2Pt^{II}]$, which is the most frequently ordered oncostatic agent in the U.S.A. Its activity is thought to be exerted, at least initially, by coordination to guanine N-7 sites on cellular nucleic acids [13]. Given the apparent parallels between the biochemical properties of *cis*-$[Cl_2(NH_3)_2Pt^{II}]$ and ruthenium ammine complexes, further studies of the latter's interactions with DNA were undertaken to determine possible molecular mechanisms for their oncological properties.

It has been demonstrated *in vitro* that reduction of $[Cl(NH_3)_5Ru^{III}]^{2+}$ is catalyzed by subcellular components of the rat liver cell [14] and by photosystem I in spinach chloroplasts [15], so that *in vivo* reduction is also likely. This should facilitate DNA binding since the aquo ligand in $[(H_2O)(NH_3)_5Ru^{II}]^{2+}$ exchanges with a half-life of about 0.1 s, which is considerably more rapid than that for the corresponding Ru^{III} complex. Moreover, the reducing, hypoxic environment prevalent in many tumors [16] should favor formation of $[(H_2O)(NH_3)_5Ru^{II}]^{2+}$. Therefore, both for convenience in synthesis and to approximate the probable *in vivo* mechanism as closely as possible, reactions were carried out with the metal ion as $[(H_2O)(NH_3)_5Ru^{II}]^{2+}$. Owing to the instability of Ru^{II}–nucleotidyl complexes with respect to air oxidation and acid catalyzed aquation, compound characterization was largely undertaken in the Ru^{III} form.

Several relatively small complexes of redox-active transition metal ions have recently been shown to cleave DNA [17]. Endonucleolytic cleavage is also featured by several metal-requiring antitumor antibiotics [18]. While the mechanism of action of these antibiotics is now the center of considerable investigation and controversy, it appears that most simple metal complexes are engaged in an autooxiation process that eventually produces hydroxy radicals, with the metal ion being recycled through its reduced state owing to the presence of a reductant. The hydroxy radicals generated proximally to the DNA are thought to attack the sugar moieties by hydrogen atom abstraction followed by sugar fragmentation and scission.

In this study we describe the extent of binding of the redox-active metal ion, $[(NH_3)_5Ru^{III}]$, to native DNA, determine the primary DNA coordination sites of this ion and, by implication, $[(H_2O)(NH_3)_5Ru^{II}]^{2+}$, detail the UV–Vis and CD spectroscopic properties of ruthenated DNA, consider the consequences of increasing amounts of covalently bound metal ions on the secondary and tertiary structure of the DNA, and delineate the effects of both free and DNA-bound Ru^{III} on the cleavage of DNA in the presence of oxygen and a reductant.

Materials and Methods

Stock solutions of $[Cl(NH_3)_5Ru^{III}]^{2+}$ were prepared by dissolving 100 mg (0.33 mmol) of its chloride salt with the addition of two equivalents of AgTFA (where TFA = trifluoroacetate) to remove the ionic chloride. The resulting solutions were adjusted to a pH of 2–3 and a final $[Cl(NH_3)_5Ru^{III}]^{2+}$ concentration of approximately 0.03 or 0.3 M. Under these conditions the complex slowly hydrolyzes to yield $[(H_2O)(NH_3)_5Ru^{III}]$; however, this has no effect on the results reported here. Reduction to $[(H_2O)(NH_3)_5Ru^{II}]^{2+}$ was carried out in an argon purged solution over Zn amalgam for 30–60 min [19].

$[(NH_3)_5Ru^{III}]_n$–DNA

Stock solutions of calf thymus DNA (Sigma, Type I) or salmon sperm DNA (Sigma, Type III) were prepared by dissolving the DNA in 0.1 M phosphate buffer at pH 7.2 or TA buffer (40 mM Tris, 5 mM sodium acetate adjusted to pH 7.8 with acetic acid) and diluting to a DNA–phosphate concentration (P_{DNA}) of 1.5 mM. Heat-denatured DNA was prepared by heating the DNA solution in a boiling water bath for 20 min and then cooling rapidly in an ice bath. Ruthenium–DNA complexes were prepared from aliquots of these solutions, which had been purged with argon for 30 min and then injected with varying amounts of the $[(H_2O)(NH_3)_5Ru^{II}]^{2+}$ solution. Reactions were allowed to proceed for 1 h at 20 °C with continuous argon bubbling. Oxidation to yield $[(NH_3)_5Ru^{III}]_n$–DNA was accomplished by a 1 h purge with O_2, which caused the initially yellow $[(NH_3)_5Ru^{II}]_n$–DNA to turn a pronounced purple color. Unreacted Ru^{III} species were removed by dialysis against the appropriate buffer or by three successive ethanol

precipitations of the DNA. Owing to slight (6–7%) loss of sample in these operations, DNA concentrations were re-determined from A_{260} and the results normalized accordingly.

Superhelical plasmid pBR322 DNA was a gift from S. Youngquist and J. Sluka and was prepared by methods similar to those of Tanaka and Weisblum [20]. A 381 base pair base pair fragment (bases −3 to 379, 26.7% G) of pBR322 DNA labeled with ^{32}P at the 3′ end was prepared by cleavage of the plasmid with BamH1 and enzymatic extension of the 3′-end with the Klenow fragment of DNA polymerase I and [α-^{32}P]dATP [21]. After a second cleavage with EcoRI, the fragment was isolated by gel electrophoresis on a 5% polyacrylamide gel [17, 22]. Superhelical pBR322 was labeled with $[(NH_3)_5Ru^{III}]$ by placing a 30 μl aliquot of the DNA ($[P_{DNA}]$ = 197 μM) in TA buffer in a 1.5 ml Eppendorf tube and deaerating for 30–45 min by bubbling water-saturated argon through a piece of #50 IP tubing inserted through a small hole in tube cap. Solutions of 200 μM, 20 μM and 2 μM $[(H_2O)(NH_3)_5Ru^{II}]^{2+}$ were prepared by reducing the more concentrated solution for 1 h over zinc-amalgam and then serially diluting this 10-fold into two 1.8 ml portions of water deaerated over zinc-amalgam. Aliquots of 3 μl were then added to the DNA solutions and the reactions allowed to continue for 100 min. A blank solution was similarly prepared by adding 3 μl of argon-purged water. Following a sufficient period for air oxidation, the DNA was checked to verify the absence of any significant DNA cleavage by agarose gel electrophoresis. The unreacted ruthenium was then removed by three dialyses in plexiglas 'button' vessels against 350 ml of TA buffer for periods of 2 h, 2 h and 10 h. Ruthenium labeling of the ^{32}P-labeled 381 bp fragment was similarly effected in 100 μl reaction volumes in the presence of CT DNA at a P_{DNA} concentration of 200 μM, with the excess ruthenium being removed by three successive ethanol precipitations of the DNA.

Physical Characterization

Ultraviolet and visible absorption spectra were determined using either a Cary 14 or a Perkin-Elmer 575 recording spectrophotometer. Spectra of 6-$[(Ado)(NH_3)_5Ru^{II}]$ were obtained by reduction of 0.1 mM solutions of this ion with a 10-fold excess of Eu^{II} in 0.1 M LiCl. Circular dichroism spectra were obtained in a 1.0 cm quartz cuvette on a Jasco J41 or Cary 60 recording spectropolarimeter equipped with a 6001 CD attachment. Ellipticities were normalized by applying the equation: $\Delta\epsilon = (\theta \times \epsilon)/(33 \times A_{258})$ [23]. Temperature melt experiments were carried out in TA buffer in a thermostatted cell programmed with a 1 °C/min temperature rise, which was monitored with a YSI-3200 thermistor temperature probe on a YSI-32 conductance/temperature meter. The output from this device and the A_{260} from the spectrophotometer were simultaneously monitored on a Houston Omnigraphic XY-recorder. Reannealling was accomplished with a 2 °C/min decrease in temperature down to 20 °C.

The binding of $[(H_2O)(NH_3)_5Ru^{II}]^{2+}$ to calf thymus DNA was monitored spectrophotometrically at 365 nm at 25 °C in either phosphate (μ = 0.1, pH 7.2) or TA buffer (pH 7.8). Reactant solutions were prepared by purging the DNA and $[Cl(NH_3)_5Ru^{III}]^{2+}$ solutions for 30–45 min by argon bubbling, with the latter containing a few pieces of zinc amalgam to reduce the ruthenium to $[(H_2O)(NH_3)_5Ru^{II}]^{2+}$. An aliquot of the Ru^{II} solution was then anaerobically transferred with continuous argon purge into a flask containing the DNA. The mixture was then anaerobically transferred into an argon-purged cuvette and sealed. Rate constants were determined from a least-squares analysis of plots of $\ln(A_\infty - A_t)$ *vs.* t over their linear portion (2 to 4 half lives).

The extent of ruthenium binding to DNA was determined by atomic absorption on a Perkin–Elmer 503 atomic absorption spectrophotometer with an HGA 2100 graphite furnace attachment or on a similar Instrumentation Laboratory Model 551 device. Standard solutions were prepared from vacuum desiccated $[(NH_3)_6Ru]Cl_3$ and were adjusted to be nearly identical in composition to the samples by adding phosphate buffer and DNA where necessary. Analysis was performed on 10 μl samples by heating the graphite oven to 110 °C over 15 s and then holding the temperature constant for an additional 5 s to dry the sample. Ashing was done by heating to 600 °C over 10 s and holding constant for 5 s, and sample atomization occurred during rapid heating to 2800 °C.

Reduction potentials of $[(NH_3)_5Ru^{III}]_n$–DNA were determined in TA buffer solutions purged with Ar or N_2 and blanketed with the gas while measurements were made. Cyclic voltammetric measurements were made on an electrochemical apparatus constructed in this laboratory [27] at scan rates of 100–300 mV/s on a platinum disk electrode with a Ag/AgCl reference and a platinum wire auxiliary electrode. Pulse voltammetric measurements were made using a PARC Model 174A polarographic analyzer with scan rates of 2 mV/s, sampling intervals of 0.5 s and a pulse height of 50 mV. Peak potential measurements were internally referenced against the $[(NH_3)_6Ru]^{3+,2+}$ couple (57 mV).

DNA Cleavage

Reactions using supercoiled pBR322 plasmid DNA (form I) as a substrate for cleavage induced by ruthenium ions in the presence of oxygen and a reductant were performed in 10 μl TA buffer at

pH 7.8. The DNA concentration was 10 μM in DNA bp. The buffer, DNA, ruthenium complex and sufficent water were premixed in an Eppendorf vial; then 2 μl of the reductant solution (5 mM dithiothreitol or ascorbate) was added and the reaction allowed to proceed for 30 min at 37 °C before addition of ficoll heading buffer and loading onto an agarose gel.

Agarose gel electrophoresis of CT DNA was performed at 50 V in 0.6% slab gels (0.4 × 10 × 12 cm) containing 0.5 μg/ml ethidium bromide. Plasmid DNA was electrophoresed at 120 V on 1% gels in TAE buffer, followed by staining in a 1 μg/ml ethidium bromide solution for 0.5 h, followed by rinsing in distilled water for 0.5 h. DNA was visualized by photographing the fluorescence of intercalated ethidium bromide under UV illumination (Ultraviolet Products C-61 Illuminator) through a Wratten 23A filter onto Polaroid Type 55 film with a Polaroid MP-4 industrial camera. Bands were quantitated by integration of the absorbance evident by scanning the Polaroid negative at 485 nm on a Cary 219 interfaced with an Apple microcomputer. Correction was then made for the decreased ethidium fluorescence in form **I** before determining the relative abundances of the three forms [24]. When only form **I** (supercoiled) and form **II** (open circular) of the DNA were present, the mean number of single-strand scissions, S, per DNA molecule was calculated assuming a Poisson (random) distribution according to the formula $S = \ln(f_{\mathbf{I}})$, where $f_{\mathbf{I}}$ is the fraction of form **I** molecules.

Reactions using the ^{32}P labeled 381 bp fragment of the pBR322 DNA were run similarly to those involving integral superhelical DNA. However, following incubation these reaction mixtures were lyophilized, suspended in 4 μl of a pH 8.3, 100 mM Tris-borate, 50% formamide loading buffer, denatured at 90 °C for 1 min and then quickly chilled in an ice bath. Electrophoresis was carried out on a 0.4 mm thick, 40 cm long, 8% polyacrylamide, 1:20 crosslinked, 50% urea gel at 1000 V until the bromphenol blue marker dye reached the bottom of the gel (4 h). Autoradiography was carried out at −50 °C on Kodak X-omat AR film.

Hydrolysis and HPLC

DNA hydrolysis was accomplished at 85 °C for 1 h after adjusting the samples to pH 1 with HCl. HPLC was performed on a Varian Model 5000 instrument fitted with a Waters μ-Bondapak C_{18} column and eluted with 0.2 M ammonium propionate at 1.5 ml/min. Details of this method together with capacity factors for various metallonucleosides and purine complexes have been published elsewhere [25]. HPLC quantitation of guanine, adenine and their $[(NH_3)_5Ru^{III}]$ complexes was determined by peak height analysis using calibration curves derived from the respective pure materials. The fraction of available guanine residues which were coordinated by the metal ion was determined by the ratio:

$$[(Gua)(NH_3)_5Ru^{III}]/([(Gua)(NH_3)_5Ru^{III}] + [G]).$$

Values for the fraction of guanines labelled determined from the chromatographic peaks represent minimum values, since some loss of compound occurred during the acid hydrolysis step. Studies with monomeric $[(dG)(NH_3)_5Ru^{III}]$ revealed an approximate 20% loss in all forms of Ru^{III}–G under the same hydrolysis conditions. Since this varied somewhat for each DNA hydrolysis, the samples for a given series of dilutions were always simultaneously prepared from the same batch of DNA and treated identically.

Results

Synthesis and Spectra

Table I summarizes the analytical results from a series of reactions involving calf thymus DNA with varying concentrations of $[(H_2O)(NH_3)_5Ru^{II}]^{2+}$ in which the reactant $[Ru^{II}]/[P_{DNA}]$ molar ratio ranged between 0.25 and 50.0. For $0.1 < [Ru^{II}]/[P_{DNA}] < 1.0$ the initially light yellow solutions grew more intense with time, indicating the formation of $[(NH_3)_5Ru^{II}]_n$–DNA [10]. Figure 1 shows the absorption spectra of one of these mixtures around 360 nm to increase substantially with time. Background spectra involving $[(H_2O)(NH_3)_5Ru^{II}]^{2+}$ and the phosphate buffer exhibited slight absorbance changes at this wavelength, which amounted to only about 3% of the corresponding DNA reactions.

A typical increase in A_{365} as a function of time is shown in Fig. 2 to undergo an initial rapid rise followed by a much lower sloping increase. Since the slower rise in absorbance continued over periods sufficiently long to allow secondary reactions owing to ammonia loss to occur, the reactions were quenched by air oxidation after 1 h. The rapid phase of the coordination reaction was complete during this period and had come close to its own equilibrium position. However, a small displacement due to binding derived from the subsequent reactions was also present, so that an approximation to equilibrium was obtained. The rate of increase of the subsequent phase was directly dependent upon $[Ru^{II}]/[P_{DNA}]$ and was almost negligible at $[Ru^{II}]/[P_{DNA}] = 0.1$ (Fig. 2), but quite significant at $[Ru^{II}]/[P_{DNA}] = 1.0$ (Fig. 1).

The major spectral changes evident in reacting $[(H_2O)(NH_3)_5Ru^{II}]^{2+}$ with DNA are the new, broad peaks in the 350–400 nm range (see Fig. 1). These absorption bands resemble the spectra for both 7-$[(Guo)(NH_3)_5Ru^{II}]^{2+}$ and $[(Ado)(NH_3)_5Ru^{II}]^{2+}$

TABLE I. Data on the Formation of $[(NH_3)_5Ru^{III}]_n$–DNA

Reaction conditions[a, b]		Precipitate[c]	A_{260}/A_{230}	A_{260}/A_{280}	l_{max} visible (nm)	Ru_{DNA}[d] (mM)	Ru_{DNA}/P_{DNA}
$[Ru]/[P_{DNA}]$	$[Ru^{II}]$ (mM)						
0.0	0.0	–	2.21	1.79	–	0.0	0.0
0.25	0.38	–	2.09	1.73	554	0.22 ± 0.02	0.14 ± 0.01
0.50	0.75	–	1.93	1.65	548	0.29 ± 0.04	0.19 ± 0.02
0.76	1.15	–	1.89	1.63	545	0.33 ± 0.04	0.22 ± 0.03
1.0	1.5	–	1.91	1.66	541	0.38 ± 0.08	0.26 ± 0.03
5.0	7.5	+					
10.0	15.0	+			484[e]		
30.0	45.0	+			475[e]		
50.0	75.0	+			476[e]		

[a]$[P_{DNA}]$ = 1.5 mM for all reactions. [b]For reactions of ratio 1.0 and lower, the final pH was found to be within 0.2 units of the initial reaction pH of 7.2. [c]Visible macroscopic brown precipitates appeared during the Ar atmosphere reaction and remained as purple precipitates following air oxidation. [d]Ruthenium bound to DNA. The average and 95% confidence range of 3 atomic absorption measurements on samples following air oxidation. [e]Undialyzed samples.

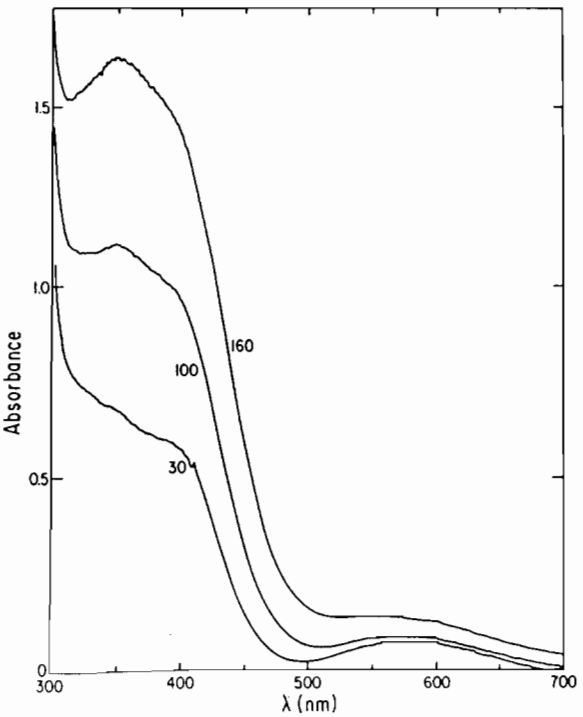

Fig. 1. Visible spectra of $[(NH_3)_5Ru^{II}]_n$–DNA (calf thymus) under Ar atmosphere. $[Ru^{II}]/[P_{DNA}]$ = 1.0, $[P_{DNA}]$ = 1.5 mM, recorded at times (min) indicated.

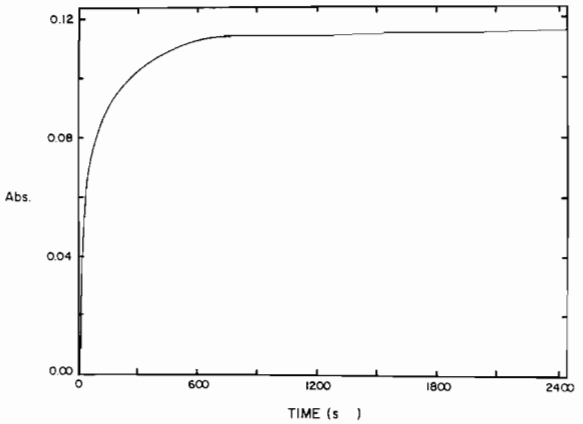

Fig. 2. Time dependency of $[(NH_3)_5Ru^{II}]_n$–DNA (calf thymus) absorbance at 350 nm $[Ru^{II}]/[P_{DNA}]$ = 0.1, $[P_{DNA}]$ = 1.5 mM, 25 °C.

(see Table II) in this region [26, 27]. A very low intensity absorption band is also apparent between 500 and 600 nm; however, owing to the extreme air sensitivity of these compounds, this feature appears to be due to a small amount of oxidation during the recording of the visible spectra (see below). Since phosphates and thymine and cytosine nucleosides do not react with $[(H_2O)(NH_3)_5Ru^{II}]^{2+}$ under these conditions to yield stable complexes, it can be concluded that the increase in absorbance in the 350–400 nm region is due to purine complexation by the metal ion. Reactions run at $[Ru^{II}]/[P_{DNA}] \geqslant 5.0$ yielded brown precipitates, which changed to purple upon air oxidation.

Oxidation of $[(NH_3)_5Ru^{II}]_n$–DNA was accomplished by bubbling air through the solutions for 1 h. The ultraviolet spectra of the resulting $[(NH_3)_5Ru^{III}]_n$–DNA samples revealed that there is little change in the intensity or shape of the $[(NH_3)_5Ru^{III}]_n$–DNA ultraviolet spectrum relative to that of free DNA. This is due to the relatively low intensity of the Ru^{III} d–d transitions in nominally octahedral complexes. For comparison, $[(NH_3)_6Ru^{III}]^{3+}$ exhibits a single electronic absorption centered at 274 nm with a molar absorptivity of only 473 M^{-1} cm^{-1}. Using this as an estimate, the contribution to

TABLE II. Spectroscopic Data for Nucleoside Complexes of $[(NH_3)_5Ru^{II}]$ and $[(NH_3)_5Ru^{III}]$ at Neutral pH

Nucleoside	Coordination site	Ru^{II}		Ru^{III}	
		λ_{max} (nm)	ϵ_{max} ($\times 10^{-3}$ M^{-1} cm^{-1})	λ_{max} (nm)	ϵ_{max} ($\times 10^{-3}$ M^{-1} cm^{-1})
Guanosine[a]	7	252	13.0	252	13.2
		365	2.1	316	1.26
				567	0.441
5′-GMP[a]	7	251	15.6	251	12.6
		370	2.4	321	1.26
				560	0.420
Adenosine[b]	1	260	8.9	unstable	
		345	1.17		
Adenosine[c]	6	unstable		251	7.8
				366	7.8
				384	8.0
				532	5.6
Cytidine[c]	4	unstable		249	7.0
				282(i)	3.4
				350	6.4
				370(s)	5.9
				471	6.99

[a]Clarke and Taube, 1974. [b]This work. [c]Clarke, 1978.

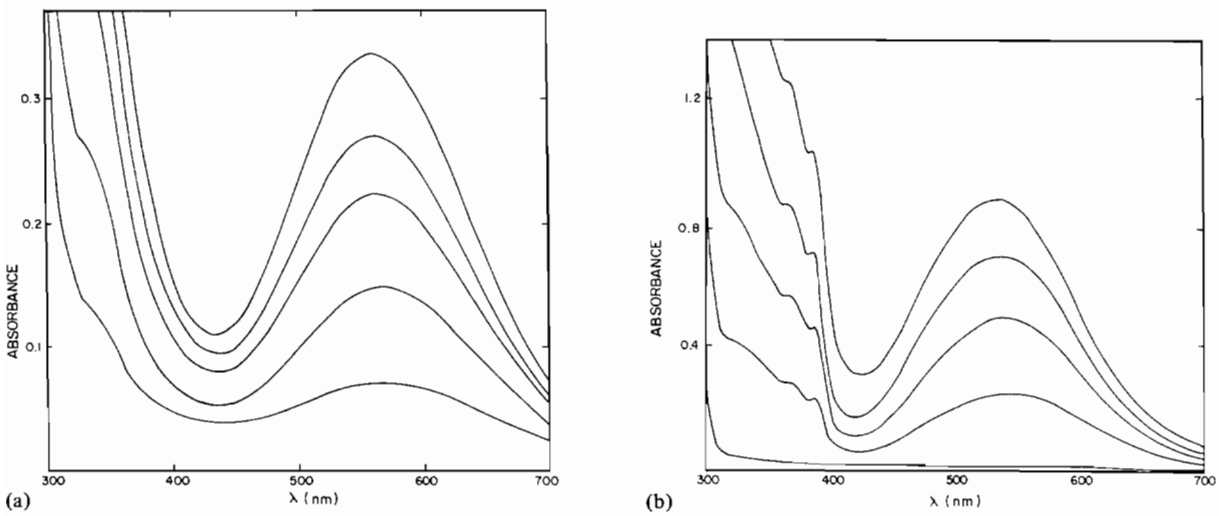

Fig. 3. (a) Visible spectra of helical $[(NH_3)_5Ru^{III}]_n$–DNA following reaction as $[(H_2O)(NH_3)_5Ru^{II}]^{2+}$ at $[Ru^{II}]/P_{DNA}] = 0.1$, 0.2, 0.35, 0.5 and 0.7 and $[P_{DNA}] = 1.5$ mM in TA buffer. Samples were air oxidized following reaction and excess ruthenium removed by 3 × ethanol precipitation. (b) Visible spectra of single-stranded $[(NH_3)_5Ru^{III}]_n$–DNA as in Fig.3a but reactions were run with heat-denatured DNA. $[Ru^{II}]/[P_{DNA}] = 0.1, 0.2, 0.35, 0.5$. Sample at $[Ru^{II}]/[P_{DNA}] = 0.7$ precipitated.

the absorption at 260 nm due to metal-only transitions is only about 4% that due to the DNA. However, at 230 nm and 280 nm the metal ion's contributions to the absorbance are measureably greater. This accounts for the noticeable decline in spectral ratios, A_{260}/A_{230} and A_{260}/A_{280}, (cf. Table I) with increasing Ru_{DNA}.

Figure 3a shows that the visible spectra of helical DNA samples prepared at $0.1 \leqslant [Ru^{II}]/[P_{DNA}] \leqslant 0.7$ exhibit a new absorption band centered around 550 nm and a disappearance of the 350 nm band evident in $[(NH_3)_5Ru^{II}]_n$–DNA. The position and bandshape of this absorption at low Ru_{DNA}/P_{DNA} are very similar to those observed in the spectrum

of $[(dG)(NH_3)_5Ru^{III}]$ under the same conditions (see Table II). Temperature melting samples of helical $[(NH_3)_5Ru^{III}]_n$–DNA resulted in an increase in A_{550} of approximately 55%.

Evidence for slow continued ruthenium binding following oxidation to Ru^{III} was noted for the samples at $[Ru^{II}]/[P_{DNA}] \leq 1$ cited in Table I. Monitoring the absorbance at 550 nm of the $[(NH_3)_5Ru^{III}]_n$–DNA samples (stored at 4 °C) revealed that the intensity of this band increased by a factor of two over a period of 7 days. Little additional change took place after this period, suggesting an approach to a different equilibrium involving $[(NH_3)_5Ru^{III}]$.

In general, spectra of $[(NH_3)_5Ru^{III}]_n$–DNA samples exhibited a shift in the visible band maxima toward higher energies together with a nonlinear increase in intensity (see Table I) with increasing $[Ru^{II}]/[P_{DNA}]$. A relative increase in the absorbance around 480 nm (which is a clear peak in several sets of spectra) and the appearance of a doublet around 360 and 380 nm occurred in all samples made with single stranded DNA (see Fig. 3b) and in some made with helical DNA, especially at high $[Ru^{II}]/[P_{DNA}]$. These new spectral features indicate that at least one additional mode of binding occurs in single-stranded DNA and at high $[Ru^{II}]/[P_{DNA}]$ in helical DNA. While the intensity of the 480 nm shoulder varied somewhat from one set of reactions to another, it was always greater at a given $[Ru^{II}]/[P_{DNA}]$ in $[(NH_3)_5Ru^{III}]_n$–DNA prepared with denatured DNA, and increased markedly with helical DNA at $[Ru^{II}]/[P_{DNA}] > 1.0$. Macroscopically, these spectral changes were accompanied by the appearance of a brownish precipitate in reactions run at $[Ru^{II}]/[P_{DNA}] \geq 5$. At $[Ru^{II}]/[P_{DNA}] > 10$ the resultant solutions prepared from helical DNA exhibited a distinct peak at 480 nm, which tended to obscure all other spectral features in the visible region.

Chromatography of $[(NH_3)_5Ru^{III}]_n$–DNA Hydrolysates

Chromatograms of acid-hydrolyzed $[(NH_3)_5Ru^{III}]_n$–DNA prepared from either helical or single-stranded calf thymus DNA were well resolved with respect to A, G and their complexes with $[(NH_3)_5Ru^{III}]$ (see Fig. 4). Chromatograms for samples prepared from helical DNA exhibit no clearly distinguishable peak for $[(Ade)(NH_3)_5Ru^{III}]$ at $[Ru^{II}]/[P_{DNA}] < 0.75$. Definite peaks for $[(Ade)(NH_3)_5Ru^{III}]$ were evident at $[Ru^{II}]/[P_{DNA}] \geq 0.15$ with denatured DNA samples. Spectroscopic investigation of bands containing the respective Ru–purine complexes, isolated both by HPLC and from bulk column chromatographies accomplished on Biorex 70 ion-exchange columns eluted with ammonium acetate buffers, revealed spectra identical to those of authentic samples of $[(Gua)(NH_3)_5Ru^{III}]$ and $[(Ade)(NH_3)_5Ru^{III}]$, respectively [3, 27]. For $0.1 < [Ru^{II}]/[P_{DNA}] \leq 0.5$ adenine and cytosine labeling was not significant for helical DNA, as indicated by the lack of a distinct HPLC peak for $[(Ade)(NH_3)_5Ru^{III}]$. At $0.1 < [Ru^{II}]/[P_{DNA}] \leq 0.75$, binding to adenine residues in single-stranded DNA appeared to remain fairly constant at $[Ru{-}A]/A_t = 0.07$, where A_t is the total available adenine residues.

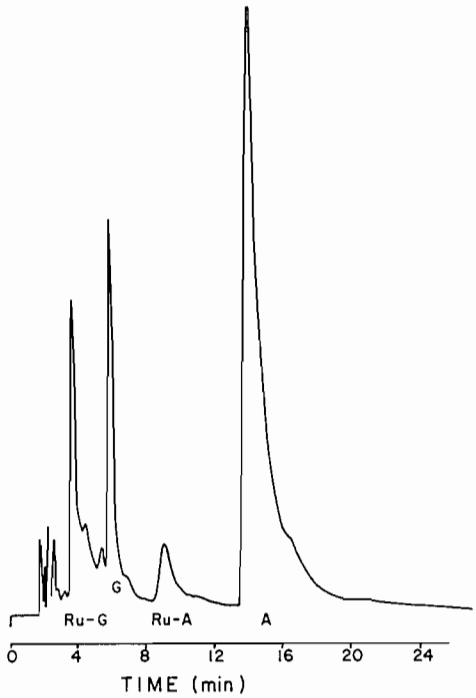

Fig. 4. Typical chromatogram of $[(NH_3)_5Ru^{III}]_n$–DNA hydrolysate prepared from heat denatured DNA for $[Ru^{II}]/[P_{DNA}] = 0.25$. Sample was eluted from a 4 mm × 300 mm octadecylsilane column with 0.2 M ammonium propionate at 1.5 ml/min.

Kinetics and Equilibria of Binding

When fitted by a standard least-squares method to the Scatchard's equation [28]:

$$\frac{[Ru{-}G]}{G_{DNA}} = \frac{R_{max}[Ru]K_{assoc}}{(1 + [Ru]K_{assoc})}$$

where R_{max} is the maximum fraction of guanine sites bound by the ruthenium, the plots of the fraction of G sites labeled as a function of $[Ru^{II}]/[P_{DNA}]$ presented in Fig. 5 yield equilibrium binding constants of: $K_{assoc} = 5.1 \pm 0.8 \times 10^3$ for helical calf thymus DNA and $K_{assoc} = 7.8 \pm 1.5 \times 10^3$ for denatured CT DNA, when corrected for loss of $[(Gua)(NH_3)_5Ru^{III}]$ in hydrolysis. Upon extrapolation to infinite $[(H_2O)(NH_3)_5Ru^{II}]^{2+}$, R_{max} is 60 ± 3% for helical DNA and 100% for single-stranded DNA. Analogous studies with helical salmon sperm DNA yielded: $K_{assoc} = 5.0 \pm 0.5 \times 10^3$ at $R_{max} = 60\%$. It

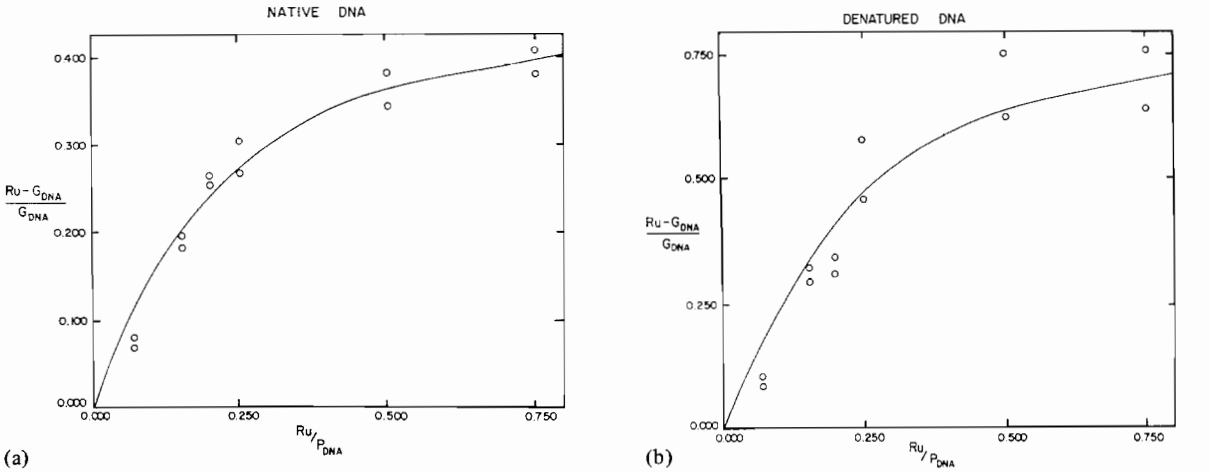

(a) (b)

Fig. 5. (a) Plot of $[(Gua)(NH_3)_5Ru^{III}]/G_{DNA}$ *vs.* $[Ru^{II}]/[P_{DNA}]$ at $[P_{DNA}]$ = 1.5 mM. Extent of ruthenium-G binding was determined by HPLC peak heights from hydrolysis of $[(NH_3)_5Ru^{III}]_n$–DNA obtained from reactions run with helical calf thymus DNA. (b) Plot of $[(Gua)(NH_3)_5Ru^{III}]/G_{DNA}$ *vs.* $[Ru^{II}]/[P_{DNA}]$ as in (a) but from samples prepared with heat-denatured, single-stranded calf thymus DNA.

TABLE III. Rates of $[(H_2O)(NH_3)_5Ru^{II}]^{2+}$ Binding to Calf Thymus DNA[a]

$[P_{DNA}]$ (mM)	[Ru] (mM)	Helical $k_{obs} \times 10^3$ (s^{-1})	Single-stranded $k_{obs} \times 10^3$ (s^{-1})
2.8	0.14, 0.07	2.4 ± 0.2	5.6 ± 0.2
1.5	0.07	2.2 ± 0.2	5.4 ± 0.2
0.7	0.035	1.8 ± 0.1	4.8 ± 0.1

[a]Reactions were run in TA buffer at 25 °C and monitored at 365 nm.

should be remembered that these estimates were made under approximately equilibrium conditions, *i.e.*, after the conclusion of the initial fast reaction and before subsequent reactions had progressed substantially, so that some systematic error is present. The data in Fig. 5 correlate well with the spectroscopic studies at low $[Ru^{II}]/[P_{DNA}]$ and show that the increase in guanine labeling for both helical and single-stranded DNA is approximately linear at $0.1 < [Ru^{II}]/[P_{DNA}] < 0.3$.

The kinetic results summarized in Table III for reactions run in TA buffer are similar to those in phosphate and indicate relatively little change with $[P_{DNA}]$. Limits imposed by metal ion precipitation of the DNA and the need for adequate absorbance changes restricted the range of reactant concentrations available; however, owing to the relatively weak dependence on $[P_{DNA}]$, rates could be determined by simple first-order methods, even at $Ru^{II}/G \geq 1/10$. While reactions could not be run in an excess of Ru^{II}, the simple exponential change in absorbance in all reactions and the invariance of the rate constant with initial ruthenium concentration strongly suggests a first-order dependence on $[(H_2O)(NH_3)_5Ru^{II}]^{2+}$. In 0.1 M phosphate buffer, observed rate constants for ruthenium binding to helical CT DNA were approximately 2×10^{-3} s^{-1} at $[P_{DNA}]$ = 1.5 mM, and the initial $[Ru^{II}]/[P_{DNA}]$ was between 0.1 and 0.5.

Metal Ion Induced DNA Structural Changes

Neutralization of 0.88–0.90 of the phosphate anionic charge by cation condensation is expected to decrease the volume of the DNA [29]. Collapse into a more compact tertiary structure was monitored by low velocity centrifugation (12 800 × *g* for 5 min), which quantitatively sediments the collapsed DNA but only a small amount of the uncollapsed fraction [30]. Application of this assay to $[(NH_3)_5Ru^{III}]_n$–DNA prepared at $[Ru^{II}]/[P_{DNA}]$ = 1.0 resulted in over 60% sedimentation, indicating that a large fraction of this sample existed in a collapsed form.

Electrophoresis of this sample in agarose gel (Lane C, supplementary Fig. 6s) showed that it neither entered the gel nor migrated. Similarly, pBR322 DNA samples incubated at $[Ru^{II}]/[P_{DNA}] \geq 1.0$ ($[P_{DNA}]$ = 20 μM) did not enter the gel at all, and at $[Ru^{II}]/[P_{DNA}] = 0.1$, $[P_{DNA}]$ = 180 μM a significant fraction did not enter. A sizeable fraction of a sample prepared by mixing $[Cl(NH_3)_5Ru^{III}]^{2+}$ with the DNA immediately prior to electrophoresis also did not enter the gel. Since $[Cl(NH_3)_5Ru^{III}]^{2+}$ has the same charge and essentially the same size and diffusion properties as $[(H_2O)(NH_3)_5Ru^{II}]^{2+}$, but cannot coordinate to the DNA on this time scale, it appears that ion-pairing sufficient to cause precipitation of the DNA occurs quite rapidly. The fraction of this sample that migrated did so with the same mobility as native DNA, suggesting that outer-sphere binding of Ru^{III} alone does not result

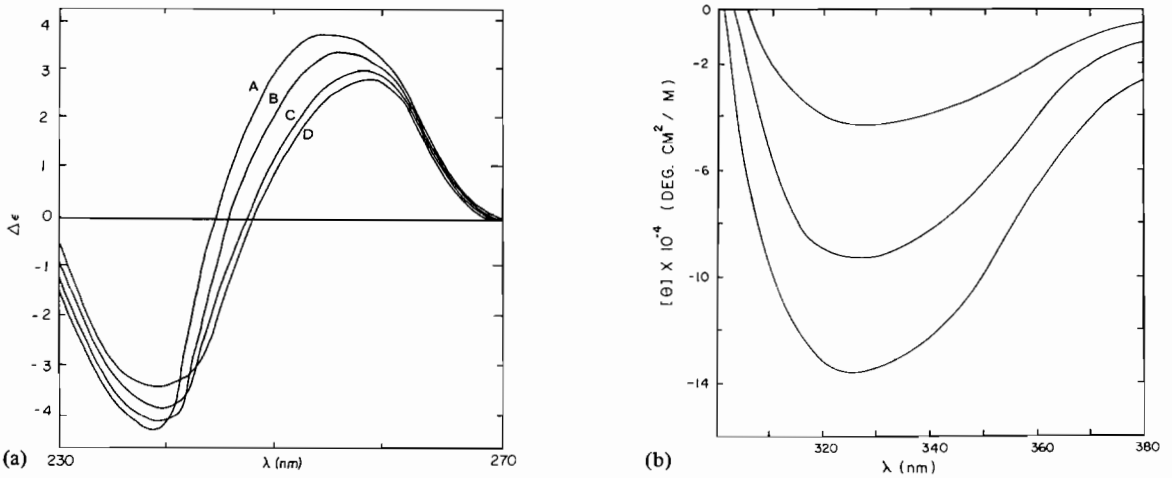

Fig. 6. (a) Normalized circular dichroism spectra of $[(NH_3)_5Ru^{III}]_n$–DNA. Samples same as in Fig. 3. A = unreacted calf thymus DNA, B, C and D = calf thymus DNA prepared at $[Ru^{II}]/[P_{DNA}]$ = 0.1, 0.35 and 0.7, respectively. (b) Detail of the circular dichroism spectra of $[(NH_3)_5Ru^{III}]_n$–DNA in the region of a G → Ru^{III} charge transfer transition at $[Ru^{II}]/[P_{DNA}]$ = 0.1, 0.35 and 0.7.

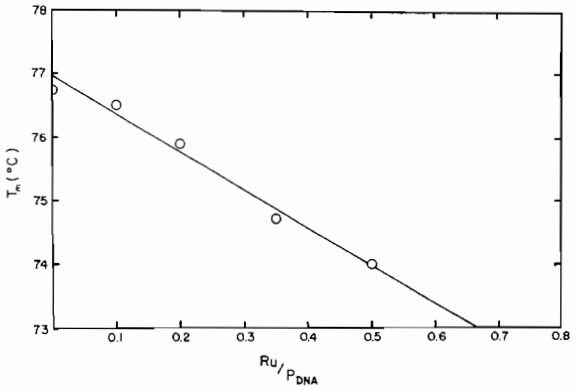

Fig. 7. Plot of T_m *vs.* $[Ru^{II}]/[P_{DNA}]$, same samples as in Fig. 3 in TA buffer.

in DNA denaturation or double stranded cleavage and that the ion can be separated from the nucleic acid during the course of the electrophoresis. In contrast, samples of pBR322 DNA, which had the ruthenium covalently coordinated, often showed a retarded mobility in electrophoresis gels.

The circular dichroism spectrum of several samples of $[(NH_3)_5Ru^{III}]_n$–DNA are shown in Fig. 6 and compared to that for unreacted calf thymus DNA. The diminution of the intensity of the CD spectra with increasing $[Ru^{II}]/[P_{DNA}]$ suggests a decrease in the helicity of the DNA; however, there is no evidence for large distortions from the native helix. Figure 6b reveals a new CD band which grows with increasing $[Ru^{II}]/[P_{DNA}]$ at 325 nm, which is in the region of a guanine to Ru^{III}, $\pi \rightarrow d_\pi$ charge transfer transition [26]. The charge transfer transition around 560 nm exhibited no CD effect.

As shown in Fig. 7, the T_m of the calf thymus DNA decreases linearly with increasing $[Ru^{II}]/[P_{DNA}]$ with a slope of −5.9 °C per unit increase in $[Ru^{II}]/[P_{DNA}]$. The temperature of onset of strand separation (defined as the temperature at which ΔA_{260} was 3% of the maximum increase in absorbance) and the amount of reannealing upon cooling were also seen to decrease with increasing $[Ru^{II}]/[P_{DNA}]$.

Electrochemistry

Electrochemical measurements by both cyclic voltammetry (CV) and differential pulse voltammetry (DPV) on $[(NH_3)_5Ru^{III}]_n$–DNA prepared from helical DNA indicated the reduction potential of the bound Ru^{III} to be 48 ± 10 mV (*vs.* SHE) in TA buffer at pH 7.8 (see Fig. 8). DPV measurements on oxidized reactant solutions and control solutions with no DNA added revealed separate peaks around 60 mV, −130 mV and −280 mV. The peak at −130 mV can be attributed to free $[OH(NH_3)_5Ru^{III}]^{2+}$. The peaks at 60 and −280 mV are due to unidentified side products, which probably contain ruthenium. The two more anodic peaks were eliminated following 3X-ethanol precipitations. Presumably, the peak at −280 mV was also eliminated, but the background current grew in this region following the ethanol precipitation, so this could not be definitely ascertained. In order to verify that the 48 mV peak exhibited by $[(NH_3)_5Ru^{III}]_n$–DNA was due to bound ruthenium, a sample of ruthenated DNA (prepared from denatured DNA) was subjected to chromatography on an SP-Sephadex column. The DPV of this sample was essentially identical to that of those subjected to ethanol precipitation only. While the CV peaks of $[(NH_3)_5Ru^{III}]_n$–DNA were relatively small compared to the background current, the forward and reverse currents appeared to be approximately equal. Since phosphate coordi-

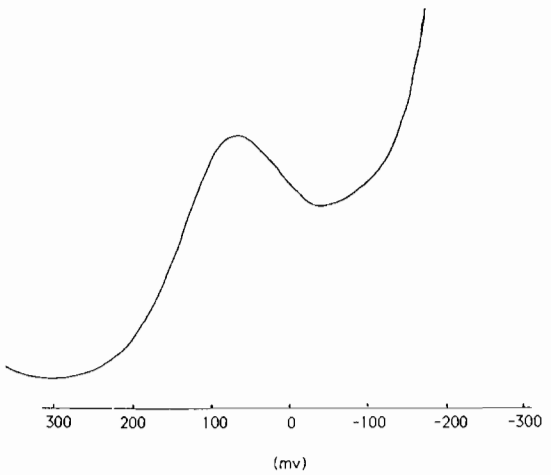

Fig. 8. Differential pulse voltammetry of denatured $[(NH_3)_5Ru^{III}]_n$–DNA in TA buffer. Scan rate 2 mV/s, pulse height 50 mV, Pt disk working electrode.

TABLE IV. Cleavage of pBR322 DNA by Ruthenium Complexes[a]

Complex	Concentration (μM)	f_I (%)	f_{II} (%)	S[b]
$[Fe(EDTA)]^-$	100	34.6	65.4	1.06
	10	82.9	17.1	0.19
$[(NH_3)_6Ru]^{3+}$	100	53.5	46.5	0.62
	10	54.6	45.4	0.60
	1	56.1	43.9	0.57
$[Cl(NH_3)_5Ru]^{2+}$	100	65.9	34.1	0.41
	10	89.5	10.5	0.11
	1	91.9	8.1	0.09
cis-$[Cl_2(NH_3)_4Ru]^+$	100	55.5	44.4	0.59
	10	79.2	20.8	0.23
	1	94.6	5.4	0.06
$[(MeHis)(NH_3)_5Ru]^{3+}$	100	76.6	23.4	0.27
	10	89.7	10.3	0.11
	1	91.8	8.2	0.09
$[dG(NH_3)_5Ru]^{3+}$ [c]	100	31.9	68.3	1.14
	10	62.1	37.9	0.48
	1	78.7	21.3	0.24
$[(Ado^-)(NH_3)_5Ru]^{2+}$ [d]	100	DNA precipitation		
	10	51.2	48.8	0.66
	1	85.1	14.9	0.16
$[(Cyd^-)(NH_3)_5Ru]^{2+}$	100[e]	15.5	84.5	1.86
	10	76.6	23.4	0.26
	1	92.3	7.7	0.08

[a]Reactions were run at 37 °C for 30 min in TA buffer, pH 7.8 with [DTT] = 1.0 mM and a DNA bp concentration of 10 μM ($[P_{DNA}]$ = 20 μM). [b]Average number of strand scissions/DNA molecule. [c]pK_a = 7.6, average charge = 2.4. [d]Polymerized sample. Polycation–polyanion interaction results in precipitation. [e]Small amount of precipitation evident.

nation was a possibility, control samples replacing DNA with glucose-6-phosphate were run. These samples exhibited no spectroscopic or electrochemical differences from those with no added ligand.

The E° potential for the metal in $[(NH_3)_5Ru^{III}]_n$–DNA is significantly less than that of $[(dG^7)(NH_3)_5Ru^{III}]^{3+}$ (E° = 0.18 V [26] or $[(5'\text{-GMP})(NH_3)_5Ru^{III}]$ (E° = 0.16 V, pH 1, E = 0.09 V in TA buffer, pH 7.8 and 0.04 V, pH 9). DPV and CV experiments on samples prepared from denatured DNA yielded similar results. Plots of DPV current *vs.* A_{560} or $[Ru_{DNA}]/[P_{DNA}]$ were linear, but of slightly varying slopes (see 'Supplementary Material'). In particular, plots of the DPV current *vs.* $[Ru_{DNA}]/[P_{DNA}]$ exhibited a positive intercept, owing to a background current in the buffer peaking at approximately 190 mV.

Cleavage of DNA by Ruthenium Complexes

Table IV summarizes the results of cleaving super pBR322 DNA in the presence of various ruthenium complexes, DTT and oxygen. All are seen to cleave the nucleic acid with an efficiency comparable to that of $[Fe(EDTA)]^-$. However, when the nucleic acid was directly coordinated by the $[(NH_3)_5Ru^{III}]$, no cleavage above background was noted under identical conditions. While the reduction potential of the metal ion is significantly lowered upon binding to DNA, reduction of $[(NH_3)_5Ru^{III}]_n$–DNA remains thermodynamically favorable in the case of DTT ($E^{\circ\prime}$ = −0.305 V) and somewhat less so for ascorbate ($E^{\circ\prime}$ = 0.06 V).

The intensity of the ethidium bromide fluorescence appeared to be decreased in DNA samples run at high ruthenium concentrations (see Fig. 7s)*. While a portion of the DNA was clearly precipitated at the higher $[Ru^{II}]/[P_{DNA}]$ and this decreased the net amount of labeled DNA migrating in the gel, fluorescence quenching by transition metal ions with spin-orbit coupling is a well known phenomenon. This interference was eliminated by probing for DNA cleavage using a ^{32}P, 3′-end labeled, 381 bp fragment with visualization effected by exposure of the polyacrylamide gel onto a photographic plate. Figure 8s* shows that the cleavage indicated by this method is also not above background. Retarded mobility and some DNA precipitation is also evident at the higher values of $[Ru^{II}]/[P_{DNA}]$, and reannealing of this DNA fragment is essentially eliminated at $[Ru^{II}]/[P_{DNA}]$ = 0.1.

Discussion

Metal Ion Binding Sites on DNA

The spectroscopic results presented in Tables I and II and in Figs. 1 and 2 indicate that $[(H_2O)$-

*'Supplementary Material'.

$(NH_3)_5Ru^{II}]^{2+}$ undergoes a fairly rapid initial reaction with helical DNA to bind to purine residues. No evidence for phosphate binding was observed, either with nucleotides or glucose-6-phosphate. While the affinity of $[(H_2O)(NH_3)_5Ru^{II}]^{2+}$ for phosphate has not been reported, it can be estimated to be considerably smaller than that for nitrogen ligands (see representative binding constants for acido ligands in ref. 19), and interactions with anionic oxygen ligands are certainly labile in this oxidation state [31, 32]. These properties allow for only transient binding of $[(H_2O)(NH_3)_5Ru^{II}]^{2+}$ to the phosphate backbone even though its polyanionic character should cause this cation to concentrate around it.

Guanine Binding

The G^7 site is established as the primary coordination site of $[(H_2O)(NH_3)_5Ru]^{2+}$ and the corresponding Ru(III) species. The coordination site of Ru^{III} following oxidation of the corresponding Ru^{II} species is usually identical to that of the lower oxidation state, whenever there are no more attractive ligands immediately impinging on an octahedral face of the metal ion [27, 33]. Such a situation holds for both $[(NH_3)_5Ru^{II}]$ and $[(NH_3)_5Ru^{III}]$ when coordinated to G^7. Synthetic studies involving the preparation of an extended series of guanine complexes with $[(NH_3)_5Ru^{II}]$ and $[(NH_3)_5Ru^{III}]$ led to the conclusion that N-7 is the binding site for both ions [26]. An X-ray structure determination of a guanine model complex, $[(Hyp)(NH_3)_5Ru^{III}]^{3+}$, which had been prepared by acid hydrolysis from the corresponding deoxyinosine complex, showed unequivocally that the metal coordination site was N-7 [33]. G^7 is readily available on the exterior of the DNA in the major groove, and molecular orbital calculations have determined this to be the most electron rich and, therefore, most favorable site for metal ion coordination in DNA [34]. Chromatography of acid hydrolysates of all types of samples of $[(NH_3)_5Ru^{III}]_n$–DNA yielded $[(Gua)(NH_3)_5Ru^{III}]$ as the major peak, which was initially identified by its chromatographic retention on both ion exchange and reverse phase columns. Further confirmation was provided by isolating the chromatographic bands containing $[(Gua)(NH_3)_5Ru^{III}]$ and verifying the compound's pK_a and electronic spectrum, both of which are sensitive to the metal ion's coordination site [33, 35].

Binding to Adenine and Cytosine

The favored coordination site for $[(NH_3)_5Ru^{II}]$ on adenosine is N-1, since this is the least sterically hindered imine nitrogen and allows for the strongest backbonding interactions [3, 27]; however, oxidation to Ru^{III} alters the mode of binding. Under physiological conditions $[(H_2O)(NH_3)_5Ru^{II}]^{2+}$ has an affinity for the N-1 site of adenosine which is a factor of 1.1×10^4 greater than that of the corresponding Ru^{III} ion. But the situation is reversed for coordination to the exocyclic amine (N-6) under the same conditions, where the affinity of Ru^{III} is 1.8×10^4 greater than that of Ru^{II} (calculated from electrochemical data given in refs. 36 and 27.

Metal ion movement from the endocyclic to exocyclic sites of adenosine has been observed to occur with a half-life of 14 s at pH 7 following oxidation to Ru^{III}, while the reverse movement proceeds with a half-life of 0.5 s following reduction to Ru^{II} [3]. At neutral pH, $[(NH_3)_5Ru^{III}]$ coordinates to the exocyclic amine of both cytosine and adenosine in their deprotonated forms (*i.e.*, to an inorganic amide, RNH^-). Proton addition at low pH, then, must occur at the adjacent pyrimidine nitrogen [27]. More recent studies have elucidated the mechanism of the N-1 to N-6 and reverse linkage isomerizations, which are a function of both the pH and the metal ion oxidation state [3].

Spectra of $[(NH_3)_5Ru^{III}]_n$–DNA prepared at $[Ru^{II}]/[P_{DNA}] > 0.3$ or with denatured DNA showed an increase in absorbance around 530 nm, where $[(Ado)(NH_3)_5Ru^{III}]$ absorbs, and often exhibited a pair of peaks around 360 and 380 nm. Reference to Table II indicates that absorbance at these wavelengths is indicative of coordination of $[(NH_3)_5Ru^{III}]$ to adenine residues. At very high $[Ru^{II}]/[P_{DNA}]$, a distinct peak was noted around 480 nm (see Table I), which is consistent with cytosine coordination of $[(NH_3)_5Ru^{III}]$. Confirmatory evidence for cytosine binding in DNA cannot be provided by the HPLC methods employed, since $[(Cyt)(NH_3)_5Ru^{III}]$ does not survive the acid hydrolysis. Nevertheless, the synthesis of this complex is effected under similar conditions so that it is reasonable to conclude that cytosine coordination takes place upon oxidation at the higher ruthenium concentrations.

Combining earlier studies with these results leads to the conclusion that while $[(NH_3)_5Ru^{II}]$ initially binds to the N-1 of adenine, it undergoes a rapid linkage isomerization following oxidation to coordinate N-6. If oxidation proceeds in the presence of unbound ruthenium, additional coordination to N-6 can occur by redox catalysis [3, 27]. While the N-3 of cytosine is similar to the N-1 of adenine, it is much more sterically hindered by the adjacent oxygen and ammine and so does not form a stable complex with Ru^{II} [3, 27, 37]. Addition of $[(NH_3)_5Ru^{III}]$ to cytosine also proceeds via redox catalysis, so that the amount of $[(NH_3)_5Ru^{III}]$ binding to A and C residues is dependent on the oxidation conditions. Reference to Fig. 3b shows that some A and C coordination occurs at all $[Ru^{II}]/[P_{DNA}]$ with single-stranded DNA. However, since the molar absorptivities of $[(Ado)(NH_3)_5Ru^{III}]$ and $[(Cyt)$-

$(NH_3)_5Ru^{III}]$ in the visible region are approximately an order of magnitude higher than those of $[(Gua)(NH_3)_5Ru^{III}]$ (cf. Table II), relatively little A and C binding has occurred even in these samples.

Equilibria of $[(H_2O)(NH_3)_5Ru^{II}]^{2+}$ Binding to G Sites

The band maxima around 550 nm in Fig. 3 arise from guanine coordination (cf. Table II). Extrapolation of the value of λ_{max} to $[Ru_{DNA}] = 0$ yields a limiting value λ_{max} of about 560 nm. Since this is very similar to that of $[(5'\text{-GMP})(NH_3)_5Ru^{III}]^{2+}$, it can be concluded that ruthenium binding to helical DNA at very low $[Ru^{II}]/[P_{DNA}]$ occurs almost entirely at the N-7 of guanine. This is confirmed by the HPLC studies which show no other significant binding at $[Ru^{II}]/[P_{DNA}] \leqslant 0.5$. The initial rapid phase of binding observed in the kinetic studies with $[(H_2O)(NH_3)_5Ru^{II}]^{2+}$ and helical calf thymus DNA applies to purine coordination by $[(NH_3)_5Ru^{II}]$. In helical DNA at low $[Ru^{II}]/[P_{DNA}]$ this is essentially limited to G^7 sites. The slower subsequent phase may involve unwinding of the DNA to allow easier access to additional sites and to interior hydrogen bonding sites on adenine and cytosine.

The binding studies done under pseudo-equilibrium conditions show that unwinding the DNA increases the fraction of guanine sites available for coordination. This implies that the coordination of $[(H_2O)(NH_3)_5Ru^{II}]^{2+}$ to helical DNA is somewhat hindered relative to single-stranded DNA. Aside from the different degrees of steric obstructions presented by the various types of adjacent base pairs, it may also be that coordination of $[(NH_3)_5Ru^{II}]$ hinders the binding of subsequent metal ions either by steric or electrostatic effects. Relative to its affinity for similar ligands such as imidazole ($K_{assoc} = 2.8 \times 10^6$) [38], the affinity of G sites in both helical and denatured DNA is decreased by a factor of about 500. On the basis of their relative affinities for protons (pK_a of imidazole = 7.4; pK_a dG = 2.4) and other metal ions, the K_{assoc} for dG is expected to be 2–2.5 orders of magnitude less than that for imidazole [39–41], so that the value obtained here is in the expected range.

Taube and Brown [42] have pointed out that the product distributions for most $[(NH_3)_5Ru^{II}]$ complexes of nitrogen heterocyles appear to be kinetically controlled. In its strictest sense, this is true here, since it was not possible to allow binding of $[(H_2O)(NH_3)_5Ru^{II}]^{2+}$ to go to completion of its biphasic kinetics. Substitution reactions of $[(H_2O)(NH_3)_5Ru^{II}]^{2+}$ usually proceed by a dissociative (SN_1) mechanism limited by the water exchange rate (5–10 s^{-1}) for this metal ion. The observed half-lives of the initial rapid binding phase of the reaction with DNA are similar to the rate calculated on the basis of the limiting water exchange rate, assuming first-order behavior in both $[(H_2O)(NH_3)_5Ru^{II}]^{2+}$ and P_{DNA}. A probable explanation for this efficiency in the kinetics of G^7 binding is that the concentration of the dispositive ion is considerably higher in the region of the polyanionic DNA. This diffusion-limited, ion-pairing equilibrium step is expected on the basis of the affinity of polyanions for oppositely charged ions and should be considered in the mechanism of DNA binding of Ru^{II} and probably all metal cations [29, 43]. A higher than expected binding rate has also been reported for the coordination of *cis*-$[(H_2O)_2(NH_3)_2Pt]$ [44], and the rapid precipitation of DNA samples by $[(H_2O)(NH_3)_5Ru^{II}]^{2+}$ and $[Cl(NH_3)_5Ru^{III}]^{2+}$ indicates that the ion-pairing process takes place quickly.

A likely reaction sequence for G^7 coordination of $[(NH_3)_5Ru^{II}]$ that accounts for the observed dependence on both $[Ru^{II}]$ and $[P_{DNA}]$ is:

$$[(H_2O)(NH_3)_5Ru^{II}]^{2+} + DNA \overset{K_{ip}}{=} [(H_2O)(NH_3)_5Ru^{II}]^{2+}\cdot DNA$$

$$[(H_2O)(NH_3)_5Ru^{II}]^{2+}\cdot DNA \underset{k_{-2}}{\overset{k_2}{\rightleftharpoons}} [(NH_3)_5Ru^{II}]\cdot DNA + H_2O$$

$$[(NH_3)_5Ru^{II}]\cdot DNA \xrightarrow[k_3]{} [(NH_3)_5Ru^{II}]\text{–}DNA$$

Since only the G^7-DNA sites are coordinated, if the DNA remains helical, the effective DNA concentration in the last step is equal to that fraction of sites which are G, *i.e.*, $[DNA]_{eff} = f_G \times P_{DNA}$. The overall rate law for this pathway is then:

$$\frac{d[Ru\text{-}G]}{dt} = \frac{f_g k_3 k_2 K_{ip}}{(k_{-2} + k_3)(1 + K_{ip}[P_{DNA}])} [P_{DNA}][Ru^{II}]$$

where k_2 is the water substitution rate on $[(H_2O)(NH_3)_5Ru^{II}]^{2+}$. K_{ip} is a function of the ionic strength of the monocations in the solution and can be estimated to be around 200 at $\mu = 0.1$ and 900 in TA buffer (calculations based on ref. 29), which leads to a concentration factor of around 500 for the metal ion in the region of the DNA.

As the product, $K_{ip}[P_{DNA}]$, approaches and becomes greater than one, which holds under these experimental conditions, the reaction begins to lose its dependency on the DNA concentration. Therefore, it is not surprising that the rate less than doubles on undergoing a four-fold increase in $[P_{DNA}]$. At higher DNA concentrations, such as occur in the nucleus, the rate should be independent of the nucleic acid concentration. Finally, it has been shown that in the absence of significant concentrations of other cations, the concentration of di- or trivalent metal ions around the polyanionic DNA does not

go to zero as the bulk concentration of these ions vanishes [29]. This leads to the prediction that at low ionic strength the rate of binding should be relatively rapid, even at low concentrations of the coordinating metal ion. Since some autoinhibition of ruthenium binding may occur owing to electrostatic effects or steric crowding, it may also be necessary to introduce an inhibitory factor, which would decrease the rate over the course of the reaction.

Binding of $[(NH_3)_5Ru^{III}]$ to G

The ion-pairing effect should be approximately the same for the analogous Ru^{III} complex since this species exists in the hydroxo form, $[(OH)(NH_3)_5Ru]^{2+}$, at neutral pH. Electrochemical measurements [1, 26] indicate that the affinity of $[(NH_3)_5Ru^{II}]$ for free guanosine is 33 times that of $[(NH_3)_5Ru^{III}]$. However, upon coordination to guanosine monophosphate, additional ion-pairing and hydrogen-bonding interactions with the phosphate can occur. Moreover, at neutral pH the metal ion can induce partial deprotonation at N-1. These effects stabilize Ru^{III} and decrease the reduction potential of $[(5'\text{-GMP})(NH_3)_5Ru^{III}]$ to only 0.095 V in TA buffer. Additional electrostatic interactions with the phosphate backbone and a possible π-effect resulting from base stacking, causing electron density to flow into the partially occupied d_π orbital on the metal ion, further reduce the reduction potential of Ru^{III} on the nucleic acid. These interactions increase the nucleic acid's relative affinity for Ru^{III} and, together with the slower binding phases previously discussed for Ru^{II}, explain the continued slow coordination of Ru^{III} for those samples allowed to stand for extended periods following oxidation of the reaction mixtures. The reduction potential of $[(NH_3)_5Ru^{III}]$ on the G^7 sites of DNA in TA buffer (0.048 V) indicates that the K_{assoc} for the Ru^{III} complex is only a factor of five less than that of $[(H_2O)(NH_3)_5Ru^{II}]^{2+}$.

G vs. A and C Binding

Brown has shown that *trans*-$[(H_2O)(SO_3)(NH_3)_4Ru^{II}]$ has an affinity for the N-7 site of guanine that is approximately 100-fold greater than its affinity for the N-1 of adenosine [42]. While this species differs significantly from $[(H_2O)(NH_3)_5Ru^{II}]^{2+}$, these workers have indicated that trend relationships between the two ions hold. This suggests that even in an idealized single-stranded DNA, where the N-1 of A and the N-7 of G are equally accessible, $[(H_2O)(NH_3)_5Ru^{II}]^{2+}$ should still exhibit a fair degree of selectivity in coordinating to G residues. This situation is especially pronounced in helical DNA, where the N-1 of A is not nearly so accessible as G^7. The steric hindrance to N-3 cytosine coordination has been previously mentioned and this mode of binding can be considered negligible for $[(NH_3)_5Ru^{II}]$.

Spectroscopic and Electrochemical Quantitation of Bound Ru^{III}

While plots of A_{560} or DPV peak height *vs.* $[Ru_{DNA}]/[P_{DNA}]$ were essentially linear, the accuracy of quantitation by either of these methods is still less than desired. Small amounts of adenine binding can occur at almost any $[Ru_{DNA}]/[P_{DNA}]$ and the resulting intense absorption centered at 530 nm can markedly affect A_{560}. Moreover, the intensities of these charge-transfer bands is increased in single-stranded regions. In the case of DPV, possible carry-over of the unidentified material exhibiting a peak at 60 mV in the reactant solution and the high buffer background make the variation in this method greater than allowed for reliable quantitation.

Cleavage of DNA upon Ru^{II} Oxidation

Oxidation of $[(NH_3)_5Ru^{II}]$ complexes of purines and pyrimidines by molecular oxygen is expected to proceed in a manner analogous to that observed for $[(\text{isonicotinamide})(NH_3)_5Ru^{II}]^{2+}$, which involves a simple bimolecular, outer-sphere oxidation of the metal ion to yield superoxide ion, followed by a second single-electron transfer from Ru^{II} to yield HO_2^- [45]. The production of superoxide ion by autooxidation of DNA-bound metal complexes has been strongly implicated as the first step in the 'Fenton's chemistry' mechanism shown to result in single-strand scission of the nucleic acid [8, 17, 46]. This mechanism ultimately produces HO•, which is thought to abstract a hydrogen atom from deoxyribose leading to sugar fragmentation, base release and DNA cleavage. Since all the ruthenium(III) complexes reported in Table IV showed at least some cleavage of pBR322 superhelical DNA, this mode of DNA disruption should be considered in possible mechanisms for the anticancer activity of ammineruthenium complexes.

Targeting the metal ion directly on the DNA was expected to yield a higher level of DNA strand cleavage than the free metal ions. Therefore, it is surprising that $[(NH_3)_5Ru^{III}]_n$–DNA did not exhibit DNA cleavage at the levels tested. While small amounts of DNA cleavage were evident in the agarose gels, this could be entirely attributed to oxidation of the Ru^{II} immediately following reaction and to general DNA damage occurring during the handling and dialyses procedures. Levels of Ru^{III} coordination were kept relatively low, in order to prevent precipitation and allow the $[(NH_3)_5Ru^{III}]_n$–DNA samples to undergo electrophoretic migration. On the basis of the results reported in Table IV for $[dG(NH_3)_5Ru]^{3+}$, it was expected that at least

0.2 strand scissions per molecule of superhelical pBR322 would occur at the highest Ru concentrations tested ($[Ru^{II}]/[P_{DNA}] = 0.1$ at $P_{DNA} = 180$ μM), where approximately 10% of the G sites or about 2% of the overall nucleotides are estimated to have been complexed. The noticeable blue color of the $[(NH_3)_5Ru^{III}]_n$–DNA, its decreased electrophoretic mobility, precipitation at higher concentrations, decreased reannealing properties, and quenching of the ethidium bromide fluorescence all verify metal ion coordination to have occurred.

Failure to observe cleavage by bound $[(NH_3)_5Ru^{III}]$ may have to do with the relatively low metal ion concentration on the DNA and steric, kinetic and/or thermodynamic effects generated by the DNA matrix. While $[dG(NH_3)_5Ru]^{3+}$ produced observable cleavage at similar $[Ru^{II}]/[P_{DNA}]$ ratios, the ion-pairing effects mentioned earlier would cause this to be substantially concentrated around the phosphate backbone on the exterior of the DNA cylinder. These ions would be mobile and freely accessible to both oxidant and reductant, which may enhance the generation of hydroxy radicals immediately adjacent to the target sugar site. Indeed, all species assumed to cleave by a Fenton's mechanism allow for some movement of the metal ion on the DNA chain. Fixing the ion on the DNA may slow the rate of its redox processes, since the approach of O_2^-, HO_2^- and the larger anionic reductants into the major groove would be sterically obstructed by adjacent bases or electrostatically hindered by the phosphate backbone. The low Ru^{III} reduction potential and the 50% increase in the absorption of the $G \rightarrow Ru^{III}$ charge-transfer transition upon DNA melting indicate the metal ion's being in a milieu significantly different from that of the bulk solution. Given these differences in its environment and accessibility, the failure of DNA-bound $[(NH_3)_5Ru^{III}]$ to cleave at low levels may be understandable.

Studies of the reactions of $[(dG)(NH_3)_5Ru^{III}]$ under physiological conditions indicate that $[(NH_3)_5Ru^{III}]$ can function (similar to alkylating agents) as a general acid in catalyzing the hydrolysis of the sugar–purine bond [47]. This suggests that coordination of $[(NH_3)_5Ru^{III}]$ to dG in nucleic acids may affect guanine loss and possibly subsequent strand cleavage. Coordination of $[(NH_3)_5Ru^{III}]$ also catalyzes autooxidation of the nucleoside to yield 8-hydroxydeoxyguanosine. Both these reactions are thought to depend upon the ability of the metal ion to polarize electron density toward it. However, the decreased reduction potential of the metal on the nucleic acid and the hyperchromicity of the $G \rightarrow Ru^{III}$ charge-transfer band on melting the DNA suggest that the Ru^{III} form is stabilized relative to the Ru^{II} and that there is a π-interaction between the metal and the extensive π-system of the DNA. Both these effects would tend to decrease the net polarization due to the metal ion and so decrease its ability to catalyze the hydrolysis and oxidation reactions. While these reactions were not observed with $[(NH_3)_5Ru^{III}]_n$–DNA, it is possible that they occur on a longer time scale and may affect the physiological behavior of ruthenium drugs.

DNA Structural Changes

The geometry of the DNA does not appear to be extensively altered or uncoiled at $[Ru^{II}]/[P_{DNA}] < 1.0$. The decrease in the CD spectrum suggests a slight unwinding of the helix, which would be expected to occur in order to accommodate the bulky metal ion within the major groove. The decreases in T_m, the temperature of onset of strand separation and the amount of reannealing of the DNA with increasing $[Ru^{II}]/[P_{DNA}]$ are also consistent with some unwinding of the helix and a degree of interference with base pairing. The new, negative band evident in the CD spectra of $[(NH_3)_5Ru^{III}]_n$–DNA samples is probably due to a $G \rightarrow Ru^{III}$ charge-transfer transition [26] with chirality imposed by the DNA helix. Unwinding of the DNA induced by the presence of a large metal ion with ammine ligands is in harmony with recent investigations showing that outer-sphere binding of ammine complexes can significantly alter DNA conformation, even to the extent of reversing the helical direction [48–50]. The occurrence of A and C binding evident in the spectroscopic studies and the presence of $[(Ado)(NH_3)_5Ru^{III}]$ in the HPLC analyses at $[Ru^{II}]/[P_{DNA}] > 0.75$ indicates the onset of helix disruption to provide single-stranded regions.

A number of light-scattering and electron-microscopic studies have shown that double-helical DNA undergoes collapse to condensed (largely torus shaped) structures by the addition of tri- or tetravalent cations [51, 52]. Coordination of the tripositive $[(NH_3)_5Ru^{III}]$ onto the exterior of the DNA must result in a lower negative axial charge density for the double helix, which should facilitate the formation of more compact tertiary structures. The sedimentation assay indicated that over 50% of the sample prepared at $[Ru^{II}]/[P_{DNA}] = 1.0$ was collapsed into a compact tertiary structure; the failure of $[(NH_3)_5Ru^{III}]_n$–DNA samples prepared at $[Ru^{II}]/[P_{DNA}] \geq 0.1$ to migrate in gel electrophoresis experiments is also consistent with irreversible collapse. Samples at relatively low Ru_{DNA}/P_{DNA} migrated with or slightly behind normal DNA.

DNA collapse occurs when the fraction (θ) of the total DNA polyanionic charge neutralized by counterion condensation reaches 0.88 to 0.90 [29, 53, 54]. Charge neutralization is sufficiently high at a reactant $[Ru^{II}]/[P_{DNA}] = 1.0$ that DNA condensation occurs upon oxidation to Ru^{III} (which increases the cationic charge by half.) For this sample (see Table I), $Ru_{DNA}/P_{DNA} = 0.258$, which translates to $\theta = 0.765$,

due solely to covalently bound metal ions; thus, only a small additional contribution to θ of 0.135 by the buffer cations is necessary for collapse of the macromolecule. Macroscopic precipitation in the Ru^{II} form did not occur until $[Ru^{II}]/[P_{DNA}] \geqslant 5$.

Conclusion

In an *in vitro* environment which mimics physiological conditions as closely as possible, reaction of $[(H_2O)(NH_3)_5Ru^{II}]^{2+}$ with helical DNA involves a relatively rapid initial coordination to G^7 sites through an ion-pair mechanism. When allowed to proceed approximately to equilibrium, the affinity for these sites is in the range expected; however, steric hindrance prevents coordination to 40% of the G sites. Increased binding to G residues neutralizes the polyanionic charge in some regions and induces DNA unwinding, strand separation and, finally, precipitation. Unwinding and/or base pair weakening facilitates metal ion attack at the additional coordination positions at N-1 A for $[(NH_3)_5Ru^{II}]$ and N-6 A and N-4 C for $[(NH_3)_5Ru^{III}]$, with binding of the latter being under catalytic control dependent upon the oxidation conditions. Autooxidation of ruthenium(II) ions regenerated by the presence of a reductant results in significant DNA strand cleavage, but this is diminished upon direct coordination of the metal ion to G^7 sites in the major groove. Further investigations will be necessary in order to determine whether (1) coordination of Ru^{II}, (2) coordination of Ru^{III}, (3) metal ion induced structural changes in the nucleic acid, (4) metal catalyzed guanine loss, (5) metal assisted guanine autooxidation, or other factors prevail in the oncological properties of ruthenium and other transition metal ions.

Supplementary Material

Available from the authors on request.

Acknowledgements

This work was supported by PHS Grants GM 26390 at Boston College and CA 23108, GM 25886 and Research Corporation grant #8859 at Dartmouth College. Early studies by M. Buchbinder and L. Plotczyk are also gratefully acknowledged. We also greatly appreciated the very helpful discussions and generous gifts of plasmid DNA from S. Youngquist, B. Iverson, J. Sluka, K. Harshman and others in the research group of Prof. Peter B. Dervan at Caltech, whom M. J. C. visited through funds from the Jasper and Marion Whiting Foundation.

References

1 M. J. Clarke, *Met. Ions Biol. Syst., 11*, 231 (1980), and refs. therein.
2 M. J. Clarke, in A. E. Martell (ed.), 'Inorganic Chemistry in Biology and Medicine', ACS Symposium Series, Vol. 190, American Chemical Society, Washington, D.C., 1980, p. 157–180.
3 M. J. Clarke, in S. J. Lippard (ed.), 'Platinum, Gold and Other Chemotherapeutic Agents', ACS Symposium Series, Vol. 209, American Chemical Society, Washington, D.C., 1983, p. 335–354.
4 R. E. Yasbin, C. R. Matthews and M. J. Clarke, *Chem. Biol. Interact., 30*, 355 (1980).
5 M. J. Clarke, *Inorg. Chem., 19*, 1103 (1980).
6 A. D. Kelman, M. J. Clarke, S. D. Edmonds and H. J. Peresie, *J. Clin. Hematol. and Oncol., 7*, 274 (1977).
7 J. R. Rubin, M. Sabat and M. Sundaralingam, *Nucl. Acid Rese., 11*, 6571 (1983).
8 J. K. Barton and E. Lolis, *J. Am. Chem. Soc., 107*, 708 (1985); J. K. Barton and A. L. Raphael, *J. Am. Chem. Soc., 107*, 2466 (1984).
9 H. Taube, *Surv. Prog. Chem., 6*, 1 (1973).
10 R. Shepherd and H. Taube, *Inorg. Chem., 12*, 1392 (1973).
11 M. J. Clarke, M. Buchbinder and A. D. Kelman, *Inorg. Chim. Acta, 27*, L27 (1978).
12 H. Taube, *Pure Appl. Chem., 51*, 901 (1979).
13 M. P. Hacker, E. B. Douple and I. H. Krakoff (eds.), 'Platinum Coordination Complexes in Cancer Chemotherapy', Nijhoff, Boston, 1984.
14 M. J. Clarke, S. Bitler, D. Rennert, M. Buchbinder and A. D. Kelman, *J. Inorg. Biochem., 12*, 79 (1980).
15 R. Barr, F. L. Crane and M. J. Clarke, *Proc. Indiana Acad. Sci., 91*, 114 (1982).
16 P. M. Gullino, *Adv. Exp. Biol. Med., 75*, 521 (1976).
17 R. P. Hertzberg and P. B. Dervan, *J. Am. Chem. Soc., 104*, 313 (1982).
18 J. C. Dabrowiak, *Met. Ions Biol. Syst., 11*, 305 (1980).
19 C. G. Kuehn and H. Taube, *J. Am. Chem. Soc., 104*, 313 (1976).
20 T. Tanaka and B. Weisblum, *J. Bacteriol., 121*, 354 (1974).
21 F. Sanger and A. R. Coulson, *J. Mol. Biol., 94*, 441 (1975).
22 A. M. Maxam and W. Gilbert, *Proc. Nat. Acad. Sci. U. S. A., 74*, 560 (1977).
23 W. Zacharias, J. E. Larson, J. Klysik, S. M. Sturdivant and R. D. Wells, *J. Biol. Chem., 257*, 2775 (1982).
24 C. W. Haidle, R. S. Lloyd and D. L. Robberson, in S. M. Hecht (ed.), 'Bleomycin: Chemical and Biochemical Aspects', Springer-Verlag, New York, (1979), p. 222.
25 M. J. Clarke, H. Perpall and K. E. Coffey, *Anal. Biochem., 122*, 404 (1982).
26 M. J. Clarke and H. Taube, *J. Am. Chem. Soc., 96*, 5413 (1974).
27 M. J. Clarke, *J. Am. Chem. Soc., 100*, 5068 (1978).
28 M. A. Howe-Grant and S. J. Lippard, *Biochem., 18*, 5762 (1979).
29 G. S. Manning, *Q. Rev. Biophys., 11*, 179 (1978).
30 K. A. Marx and T. C. Reynolds, *Biochem. Biophys. Acta, 741*, 279 (1983).
31 J. A. Marchant, T. Matsubara and P. D. Ford, *Inorg. Chem., 16*, 2160 (1977).
32 J. A. Stritar and H. Taube, *Inorg. Chem., 8*, 2281 (1969).
33 M. E. Kastner, K. F. Coffey, M. J. Clarke, S. E. Edmonds and K. Eriks, *J. Am. Chem. Soc., 103*, 5747 (1981).

34 S. P. McGlynn, D. Dougherty, T. Mathers and S. Adulner, in B. Pullman and N. Goldblum (eds.), 'Excited States in Organic Chemistry and Biochemistry', Reidel, Dordrecht, 1977, p. 247–256, and refs. therein.
35 M. J. Clarke, *Inorg. Chem., 16*, 738 (1977).
36 M. J. Clarke, *Rev. Inorg. Chem., 2*, 27 (1980).
37 B. J. Graves and D. J. Hodgson, *J. Am. Chem. Soc., 101*, 5608 (1980).
38 R. J. Sundberg, R. F. Brian, I. F. Taylor and H. Taube, *J. Am. Chem. Soc., 96*, 381 (1974).
39 S. H. Kim and R. B. Martin, *Inorg. Chim. Acta, 91*, 19 (1984).
40 R. B. Martin and Y. H. Mariam, *Met. Ions Biol. Syst., 8*, 57 (1979).
41 R. B. Martin, *Acc. Chem. Res., 18*, 32 (1985).
42 G. M. Brown, J. E. Sutton and H. Taube, *J. Am. Chem. Soc., 100*, 2767 (1978).
43 M. Daune, *Met. Ions Biol. Syst., 3*, 1 (1977).
44 N. P. Johnson, J. D. Hoeschele and R. O. Rahn, *Chem. Biol. Interact., 30*, 151 (1980).
45 D. Stanbury, O. Haas and H. Taube, *Inorg. Chem., 19*, 518 (1980).
46 R. P. Hertzberg and P. B. Dervan, *Biochemistry, 23*, 3934 (1984).
47 M. J. Clarke and P. E. Morrissey, *Inorg. Chim. Acta, 80*, L69 (1984).
48 G. L. Eichhorn, Y. A. Shin, J. J. Butzow and B. F. Hughes, *Biophys. J., 37*, 333A (1982).
49 D. C. Rau and E. Charney, *Biophys. J., 37*, 292a (1982).
50 M. Behe and G. Felsenfeld, *Proc. Nat. Acad. Sci. U.S.A., 78*, 1619 (1981).
51 K. A. Marx and G. C. Ruben, *Nucleic Acid Res., 11*, 1839, 1853 (1983); K. A. Marx and G. C. Ruben, *J. Biomolecular Struct. Dynamics, 1*, 1109 (1984); K. A. Marx and G. C. Ruben, in R. Rein (ed.), 'The Molecular Basis of Cancer', 172A, Alan R. Liss, New York, 1985, p. 131, and refs. therein.
52 S. A. Allison, J. C. Herr and J. M. Schurr, *Biopolymers, 20*, 469 (1981).
53 J. Widom and R. L. Baldwin, *J. Mol. Biol., 144*, 421 (1980).
54 R. W. Wilson and V. A. Boomfield, *Biochem., 18*, 2192 (1979).